Published by IMechE Part H: Journal of Engineering in Medicine (2011; 225 (H1): 25-37)

Transient elastohydrodynamic lubrication analysis of a novel metal-on-metal hip prosthesis with a nonspherical femoral bearing surface

Qingen Meng*, Feng Liu, John Fisher, Zhongmin Jin

Institute of Medical and Biological Engineering,

School of Mechanical Engineering,

University of Leeds, Leeds,

LS2 9JT, UK

* Corresponding author

Tel: 44 113 343 8893

Fax: 44 113 242 4611

Email: Q.Meng@leeds.ac.uk

Abstract:

Effective lubrication performance of metal-on-metal hip implants only requires optimum conformity within the main loaded area, while it is advantageous to increase the clearance in the equatorial region. Such a varying clearance can be achieved by using nonspherical bearing surfaces for either acetabular or femoral components. An elastohydrodynamic lubrication model of a novel metal-on-metal hip prosthesis using a nonspherical femoral bearing surface against a spherical cup was solved under ISO standard specified dynamic loading and motion conditions. A full numerical methodology of considering the geometric variation in the rotating nonspherical head in elastohydrodynamic lubrication solution was presented, which is applicable to all non-spherical head designs. The lubrication performance of a hip prosthesis using a specific nonspherical femoral head, Alpharabola, was analyzed and compared with those of spherical bearing surfaces and nonspherical Alpharabola cup investigated in previous studies. The sensitivity of the lubrication performance to the anteversion angle of the Alpharabola head was also investigated. Results showed that the nonspherical head introduced a large squeeze film action and also led to a large variation in clearance within the loaded area. With the same equatorial clearance, the lubrication performance of the metal-on-metal hip prosthesis using an Alpharabola head was better than that of the conventional spherical bearings while worse than that of the metal-on-metal hip prosthesis using an Alpharabola cup. The reduction in the lubrication performance caused by the initial anteversion angle of the nonspherical head was small, compared with the improvement resulted from the nonspherical geometry.

Keywords: metal-on-metal hip prostheses, elastohydrodynamic lubrication, nonspherical bearing surfaces, Alpharabola surface, initial contact position

1. INTRODUCTION

While the long term adverse biological effects of metallic wear particles on patients receiving metal-on-metal (MOM) hip prostheses are still unknown, it is clear that the number of the metallic wear particles is very large and they are of nanometer size [1, 2]. These particles are very likely to be absorbed by the joint tissues and disseminated to other organs, resulting in an increase in metal ion level [3–6]. The concerns raised by exposing to the metal ions include hypersensitivity, tissue toxicity, carcinogenicity and DNA damage [7–9]. Therefore, in order to avoid the potential risk of adverse biological reactions caused by the metallic particles, it is necessary to minimize the wear of MOM hip prostheses through optimizing designs which enhance lubrication.

Current MOM hip prostheses typically consist of a spherical femoral head articulating against a hemispherical acetabular cup of a slightly larger diameter. These spherical MOM bearings exhibit an initial running-in or bedding-in phase with a higher wear rate, followed by a steady-state phase with a lower wear rate [10–12]. During the running-in wear phase, the two bearing surfaces of hip prostheses are slowly modified by wear, forming more conforming bearing surfaces within the worn area [13–16]. Within the worn patch, the clearance between the two bearing surfaces is significantly reduced, compared with the initial value. This produces a more conforming geometry of which the gap varies more gradually. Such a gap reduces the pressure gradient at the inlet, resulting in the reduction in the Poiseuille flow. As a result, more lubricant is allowed to flow into the main loaded area to improve lubrication. Therefore, the worn geometry after the running in wear is more favorable to fluid film lubrication [12, 14]. When fluid film lubrication prevails, the stead-state wear phase occurs at a lower rate. Therefore, the presence of the running-in wear phase implies that spherical

bearings are not optimal for MOM hip prostheses. The optimal bearing surfaces for MOM hip prostheses should resemble those of the worn bearing surfaces after the running-in period, with closer conforming surfaces.

In spherical MOM bearings, closer conforming surfaces can be produced by using a smaller radial clearance. Previous studies [11, 17–19] have shown that a smaller clearance is preferable to enhance lubrication and minimize wear. However, a drastic increase in wear and frictional torque resulted from an excessively small clearance has also been seen [20, 21]. Moreover, the reduction in clearance is limited by a number of practical factors. A reduction in clearance results in an increase in the contact area and it is important to ensure that the contact area is still confined within the bearing surface to avoid edge contact, particularly when the anatomical position of the cup is considered. A smaller clearance also requires a higher manufacturing accuracy in terms of reducing the non-sphericity and improving the surface finish of the bearing surfaces. It is also important to consider the potential clamping and equatorial contact under loading and when prostheses are put in through press-fit [22].

Therefore, it is only necessary to minimize the clearance of the MOM bearings within the main loaded area to obtain a larger conforming region, while it is advantageous to increase the clearance in the equatorial region to avoid the potential adverse factors. Such a variable clearance can be achieved through using aspherical bearing surfaces for either acetabular cups or femoral heads. The dry contact mechanics, steady-state and transient lubrication analyses of a novel MOM hip prosthesis employing an Alpharabola acetabular cup have been investigated [23, 24]. Significant improvement in film thickness from the Alpharabola cup was predicted under both steady-state and transient walking conditions. This is consistent

with a previous experimental study [25], in which the running-in wear between a worn acetabular component after 5×10^6 cycles and a replaced pristine head was reduced.

This is also possible to use a nonspherical femoral head. DePuy's aSphere^{TM} is designed to have a radius of curvature in the articulation zone (smaller clearance) larger than the radius of curvature elsewhere. Such a design has been shown to produce exceedingly low wear rates and ion release compared with the conventional spherical bearing couples [26]. Based on the similar concept, there are a few other non-spherical designs [27, 28], among which is Alpharabola surface. Through choosing appropriate parameters for one single function, the Alpharabola femoral head can form a large conforming area at the loaded region and a large equatorial clearance. Therefore, it can be expected to promote lubrication comparing with a spherical bearing with similar equatorial clearance. However, the lubrication of a nonspherical femoral head under realistic conditions can be quite complex, since the motion of a nonspherical femoral bearing surface not only changes the local clearance at the loaded area but also introduces additional squeeze-film action. Such a complex and important problem, particularly using the Alpharabola bearing surface for the femoral head, has not been tackled in the previous literature. The purpose of this study was to investigate the transient elastohydrodynamic lubrication (EHL) of a novel hip prosthesis using an Alpharabola head under the dynamic load and motion conditions specified by ISO standard. Most importantly, the numerical method developed in the present study, incorporating the rotation of the nonspherical geometry of the head in the EHL analysis of hip implants, is applicable to other non-spherical head designs.

2. MODEL AND METHODS

A MOM hip prosthesis consisting of a cobalt-chromium (CoCr) metallic spherical cup articulating against a nonspherical head with the same material was studied in the present study. The spherical cup was assumed to have a diameter of 28 mm and a thickness of 9.5 mm. Since the inclination of the cup has a negligible effect on the EHL under steady walking conditions [29], the cup was positioned horizontally instead of anatomically with an angle of 45°. The fixation of the acetabular cup is usually achieved either with or without cement. Cement can provide a mechanical interlock into the cancellous bone and surface structure on the back side of the cup. If the cementless method is used, the primary stability is achieved by press-fitting while the long term secondary fixation is reached by the in-growth of bone to the implant surface. In this study, the bone and the fixation of the cup were represented by an equivalent support layer with a thickness of 2 mm and appropriate mechanical properties [30]. A Cartesian coordinate system (x, y, z), shown in Figs. 1 and 3, was fixed on the cup. When the rotation angle of the head was zero, the surface of the nonspherical head was given by equation (1):

$$\frac{x^2}{R_1^2/\alpha}+\frac{\left(y-R_1+R_1/\alpha\right)^2}{R_1^2/\alpha^2}+\frac{z^2}{R_1^2/\alpha}=1,\ \alpha>1 \tag{1}$$

where R_1 is the desired maximum radius of curvature of the head; α is a parameter to control the variation rate of the radius of curvature. The maximum radius of curvature of the head (R_1) was specified to be the same as the radius of the cup, R_2, to produce a local zero radial clearance at the pole while a large equatorial clearance when the rotation angle of the head was zero.

The lubricant in artificial hip joints is periprosthetic synovial fluid, which behaves as a powerful non-Newtonian fluid under relatively low shear rates. However, it becomes Newtonian, isoviscous and incompressible at higher shear rates (10^5/s) as experienced in hip

joints during normal walking [31–33]. Therefore a realistic viscosity of 0.002 Pa s was adopted to simulate the *in-vivo* conditions [32]. The important geometric and mechanical parameters of the transient EHL models of MOM hip prostheses using Alpharabola heads adopted in this study are summarized in Tables 1.

In reality, both the load and motion experienced by human hip joints are three-dimensional and time-dependent [34]. Since the resultant load is in the direction of about 10° medially to the vertical axis and the major velocity component is in the flexion/extension direction [34], only the vertical load component, w_y, and the rotation velocity around the z axis, ω_z, were considered. Different patterns of load and velocity have been used to represent the complex walking conditions in hip joints [35]. In this study, the walking conditions specified by the ISO 14242-1 testing standard [36], shown in Fig. 2, were adopted.

The governing equations for the EHL analysis included the Reynolds, the film thickness and the load equivalent equations. The Reynolds equation governing the hydrodynamic action between the two bearing surfaces of the hip prosthesis took the following form in spherical coordinates for the present study:

$$\sin\theta\frac{\partial}{\partial\theta}\left(h^3\sin\theta\frac{\partial p}{\partial\theta}\right)+\frac{\partial}{\partial\phi}\left(h^3\frac{\partial p}{\partial\phi}\right)=6\eta R_2^2\sin^2\theta\left(\omega(t)\frac{\partial h}{\partial\phi}+2\frac{\partial h}{\partial t}\right) \qquad (2)$$

where p is the hydrodynamic pressure; h is the film thickness; η is the viscosity of the periprosthetic synovial fluid; t is time; ω is the angular velocity of the femoral head; ϕ and θ are spherical coordinates, as defined in Fig. 3. The boundary conditions for the Reynolds equation at any instant were:

$$p(0,\theta)=p(\pi,\theta)=p(\phi,0)=p(\phi,\pi)=0$$

$$\partial p/\partial\phi=\partial p/\partial\theta=0\,,\ 0<\phi<\pi\,,\ 0<\theta<\pi$$

The film thickness equation consisted of the undeformed gap formed by the bearing surfaces and the elastic deformation of the surfaces due to the hydrodynamic pressure:

$$h = R_2 - R_{\mathrm{h}}(t,\theta,\phi) - e_x \sin\theta\cos\phi - e_y \sin\theta\sin\phi + \delta \tag{3}$$

where R_{h} is the varying radius of the aspherical head; e_x and e_y are the eccentricities of the femoral head; δ is the elastic deformation of the bearing surfaces.

The external load components were balanced by the integration of the hydrodynamic pressure:

$$f_x = R_2^2 \int_0^{\pi}\int_0^{\pi} p \sin^2\theta \cos\phi \, d\theta \, d\phi = 0$$

$$f_y = R_2^2 \int_0^{\pi}\int_0^{\pi} p \sin^2\theta \sin\phi \, d\theta \, d\phi = w_y(t)$$

$$f_z = R_2^2 \int_0^{\pi}\int_0^{\pi} p \sin\theta \cos\theta \, d\theta \, d\phi = 0 \tag{4}$$

The details of the numerical method to solve the above governing equations have been given elsewhere [24, 37]. In brief, the governing equations were non-dimensionalised to facilitate the numerical analysis and improve the stability of the numerical process. A walking gait was divided into 100 instants. At each instant, the Reynolds equation was solved using a multi-grid method, while the elastic deformation was calculated using a multi-level multi-integration technique [38]. Three levels of grid were used in the multilevel solver. On the finest level, 257 nodes were arranged in both the θ and ϕ directions [39]. The load balance was satisfied through adjusting the eccentricities of the head according to the calculated load components from the hydrodynamic pressure.

Besides the variation in the load and rotation velocity experienced by the hip prostheses, the varying geometry of the head is another independent time-dependant variable that also

contributes to squeeze-film action. At each instant, the radial distance of each node on the surface of the head, $R_h(t, \theta, \phi)$ in equation (3), was calculated as detailed below.

The mesh of the spherical coordinates was set on the cup. A local reference coordinate system (x', y', z') was fixed on the head. This reference coordinate system was coincident with the fixed coordinate system when the rotation angle of the head was zero. In this way, the geometry equation of the head at each instant and rotation angle remained the same in the reference coordinate system:

$$\frac{x'^2}{R_1^2/\alpha} + \frac{\left(y' - R_1 + R_1/\alpha\right)^2}{R_1^2/\alpha^2} + \frac{z'^2}{R_1^2/\alpha} = 1,\ \alpha > 1 \tag{5}$$

The geometry equation of the head in the fixed coordinate system was obtained by transferring equation (5) using the Euler angular transformation:

$$\begin{Bmatrix} x \\ y \\ z \end{Bmatrix} = T_{2,1} \begin{Bmatrix} x' \\ y' \\ z' \end{Bmatrix} \tag{6}$$

where $T_{2,1}$ is the similarity transformation from the reference frame to the fixed frame, in the following form for the present study:

$$T_{2,1} = \begin{bmatrix} \cos(-\gamma_z) & \sin(-\gamma_z) & 0 \\ -\sin(-\gamma_z) & \cos(-\gamma_z) & 0 \\ 0 & 0 & 1 \end{bmatrix} \tag{7}$$

where γ_z is the rotation angle. It should be pointed out that if complex motions of internal/external and abduction/adduction are considered, the above method is still valid by using corresponding Euler angles.

After the geometry equation of the head in the fixed coordinate system was solved, the following equations:

$$x = R_h \sin\theta \cos\phi,\ y = R_h \sin\theta \sin\phi, \text{ and } z = R_h \cos\theta \tag{8}$$

were substituted into this geometry equation. The radius of curvature of the head at each node, $R_h(t, \theta, \phi)$, was calculated by solving the resultant quadratic equation with R_h as unknowns.

The lubrication performance of the hip prosthesis using the Alpharabola head was compared with those of the conventional spherical bearing and the hip prosthesis using an Alpharabola cup. The modes of lubrication of the three types of hip prostheses were predicted based on the lambda ratio, which is defined as

$$\Lambda = \frac{h_{min}}{\sqrt{R_{a(head)}^2 + R_{a(cup)}^2}} \tag{9}$$

where h_{min} is the minimum film thickness during a walking cycle; $R_{a(head)}$ and $R_{a(cup)}$ are average roughness of the femoral head and acetabular cup respectively, typically in the range between 5 and 15 nm [40]. The larger value of the roughness, 15 nm, resulting in a composite surface roughness of 21 nm, was adopted in this study to estimate the worse case scenario.

The sensitivity of the lubrication performance to the initial implantation position of the Alpharabola head was also investigated. This was studied by specifying an initial rotation angle between –5° and 5° in the entraining direction for the Alpharabola head.

3. RESULTS

Fig. 4 shows the variation in the minimum and central film thicknesses and the maximum pressure of an Alpharabola head hip prosthesis within four walking cycles. Although there

are three independent time-dependant variables in present study, cyclic convergent solution was obtained after three cycles. Results shown in Figs. 5–9 were taken from the fourth walking cycle when the cyclic convergence was achieved. The typical profiles of lubricant film and hydrodynamic pressure of an Alpharabola head hip prosthesis at the instants of 0.1 s, 0.3 s and 0.58 s are shown in Fig. 5. The detailed variation in the film thickness and pressure distribution at the central line along the entraining direction in one normal walking gait is elaborated in Fig. 6 for an Alpharabola head hip prosthesis. In order to explain the effect of the nonspherical geometry of the head on the lubrication performance, Fig. 7 shows the variations in the radial clearance between the cups and the heads for two nonspherical designs at the centre of the cups ($\theta = \pi/2$, $\phi = \pi/2$) in one walking gait. Fig. 8 compares the central and minimum film thicknesses and the maximum pressure between MOM hip prostheses with an Alpharabola cup, an Alpharabola head and spherical bearing surfaces. The effect of anteversion angles of 5° and –5° of the Alpharabola head on lubrication performance is shown in Fig. 9.

4. DISCUSSION

The film thickness in MOM hip prostheses is mainly determined by the initial gap between the cup and head, particularly the inlet gap, and the elastic deformation of the bearing surfaces. For the hip prostheses using a nonspherical head, the initial undeformed gap was time-dependant due to the rotation of the nonspherical head. Moreover, the time-dependent load and motion resulted in transient hydrodynamic pressure and elastic deformation as well. All these contributed to a significant squeeze-film action and influenced the predicted film thickness and pressure in a complex manner for the Alpharabola head prosthesis, as shown in Figs. 5 and 6.

The nonspherical head generated two effects on the lubrication. Firstly, it produced additional squeeze film action due to the change of geometry. However, because of the complex kinematic conditions experienced as well as the potential synergistic effect, it is difficult to specify the individual contributions of the load, velocity and geometry to the squeeze film action. Nevertheless, it is clear that at about 0.2 s when the load was decreasing and the velocity was increasing, both providing a separation effect, the film thickness at the inlet became significantly thicker due to the squeezing effect caused by the geometric variation, as observed from Fig. 6. Furthermore, at the instant of 0.4 s, both the radial clearances at the main loaded area and the walking conditions of the Alpharabola head and Alpharabola cup prostheses were similar. However, the central film thickness of the Alpharabola head prosthesis was thicker than that of the Alpharabola cup prosthesis as shown in Fig. 8a. This is another evidence of the squeeze film action caused by the geometric variation of the nonspherical head.

Secondly, the rotation of the nonspherical head resulted in a variable clearance at the loaded area. As shown in Fig. 7, for the case of $\alpha = 1.01$, the radial clearance at the centre position of the cup ($\theta = \pi/2$, $\phi = \pi/2$) varied from zero to 0.6 μm. The effect of this radial clearance on the hydrodynamic pressure can be highlighted by only considering the swing phase (0.6 s – 1.0 s) when the external load remained constant. Normally, the hydrodynamic pressure is mainly determined by the bearing geometry and the external load. For the spherical bearing surfaces and the Alpharabola cup, if the geometric parameters are given, the hydrodynamic pressure is largely determined by load. Therefore, during the swing phase, the hydrodynamic pressure remained nearly constant as shown in Fig. 8c for both cases. For the Alpharabola head prosthesis, however, the contact area decreased during this stage with the increase in the

clearance at the loaded area, as shown in Fig. 6. The hydrodynamic pressure thereby increased as shown in Fig. 8c. The effect of this variable clearance on the film thickness can be shown by examining the variation in the predicted central film thickness again. At the instants of 0.3 s and 0.68 s, the zero clearance was achieved within the loaded conjunction, resulting in a most conforming area there. Therefore, the effect of the squeeze film action on the central film thickness was very strong at the instants of 0.4 s and 0.7 s because of the well known time lag of the squeeze film action, as shown in Figs. 6 and 8a. At other instants, the action of the squeeze film action was not as strong as at 0.4 s and 0.7 s because of the effect of the increased clearance.

As shown in Fig. 7, when the zero clearance was not within the loaded area, the clearance of the nonspherical head prosthesis with a larger α at that region was larger than that of the prosthesis with a smaller α. The conforming area of the head with α = 1.01 was therefore smaller than that of the head with α = 1.0043. Consequently, the central and minimum film thicknesses of the head with α = 1.0043 were thicker than those of the head with α = 1.01, while the maximum pressure was lower, as shown in Figs. 4 and 8. This is consistent with the well recognised conclusion for the spherical bearings [17–19]. However, it should also be noted that a larger α produces a larger equatorial radial clearance, which is important to avoid the potential clamping and equatorial contact. Therefore, an optimum design of Alpharabola head requires balanced consideration of the geometric parameters.

The lubrication performances of the hip prostheses using spherical bearing surfaces, Alpharabola cup and Alpharabola head are compared by assuming a similar equatorial radial clearance. The equatorial radial clearance of the Alpharabola head prosthesis was calculated when its rotation angle was zero. The corresponding α value was approximately 1.0043 for

the Alpharabola head prosthesis to produce an equatorial radial clearance of 30 μm as used in the spherical bearing surfaces. It is clear as shown in Fig. 8 that during most of the walking cycle, the central film thickness for the Alpharabola head prosthesis was more than three folds of that of the spherical bearing. The minimum film thickness of the Alpharabola head prosthesis was significantly improved compared with the spherical bearing, especially during the swing phase. On the other hand, when the nonspherical head was compared with the nonspherical cup, a similar central film thickness was generated from 0.3 s to 0.7 s as discussed above. However, during other time periods, the predicted film thickness for the nonspherical head was considerably smaller than that of the nonspherical cup. Nevertheless, the predicted lambda ratio suggests that both the Alpharabola head and Alpharabola cup prostheses should benefit from fluid film lubrication during the whole walking gait, while the spherical bearing may only experience fluid film lubrication during 10% of the walking cycle. Similar conclusions were also reached for the maximum pressure. The maximum pressure of the Alpharabola head prosthesis was only 1/3 of that of the spherical prosthesis during most of a walking cycle, and was however about 70 % higher than that of the Alpharabola cup prosthesis at the peaks of the load (0.1 s and 0.5 s).

The inclination and anteversion angles resulted from the implantation have direct effects on the position of the zero clearance and may prevent the optimum lubrication performance. It is therefore necessary to investigate the lubrication sensitivity of the lubrication performance of the nonspherical head with respect to the initial contact position. As shown in Fig. 9, although the maximum differences in central and minimum film thicknesses and maximum pressure caused by an anteversion angel of 5° were 31.6%, 32.4% and 28.7% respectively, the film thicknesses of the Alpharabola head were still much higher than those of the spherical bearing, while the maximum pressure much lower. Moreover, since the pole of the

nonspherical head passed the main loaded region twice during a flexion/extension gait, the effect of geometrical variation was averaged. Therefore, the lubrication performance of the nonspherical head can be expected to have a less dependence on the initial position, compared with the Alpharabola cup prosthesis, in which the optimum contact position of the nonspherical cup may always be out of the loaded area.

It should be noted that MOM bearings operate in a mixed lubrication mode, where both fluid film and boundary layer can act to reduce wear. Enhanced film fluid film thickness and entrainment not only reduce the solid to solid contact and hence wear, but also entrain more serum protein into the contact which has the potential to replenish the complex protein boundary layer on the metal surface so reducing friction and reducing mechanical and corrosion wear.

However, the present predictions on the Alpharabola head need to be tested experimentally using hip simulators in future work. Moreover, besides the orientation of components during implantation investigated in this study, the complex hip joint motion during daily activities may also have important effect on the lubrication optimisation of this novel hip implant. Therefore, the sensitivity of the lubrication to different activities, such as climbing and going down stairs, rising from sitting, etc., will also be investigated. It should also be pointed out that although the clearance was focused in the present study, it is the local geometry at the inlet of the lubricated conjunction that is mainly responsible for the predicted lubricant film thickness. However, such geometry may be difficult to design since the inlet location depends on the load which is time dependent during walking. More importantly, since the method developed in the present study is generic, a number of other recently proposed non-spherical

designs for the femoral heads [27, 28, 41] can be examined to provide better understanding of how the local geometry of the bearing surfaces can influence lubrication.

4. CONCLUSION

A methodology of incorporating the nonspherical geometry of a rotating head was presented, which is applicable to all the nonspherical head designs. The transient EHL of a novel hip prosthesis using an Alpharabola head was investigated under dynamic load and motion specified by ISO standard using the new developed method. The lubrication mechanism of the hip prosthesis using Alpharabola head was analyzed. The lubrication performances of the hip prostheses using spherical bearing surfaces, Alpharabola cup and Alpharabola head were compared. The following conclusion can be drawn from the present study:

1. The lubrication mechanism of the MOM hip prostheses using nonspherical head was very complicated because the nonspherical head not only introduced additional squeeze film action but also resulted in a variable clearance at the loaded area.

2. Compared with the spherical bearing with the same equatorial radial clearance, the film thickness of the Alpharabola head was significantly increased while the maximum pressure significantly decreased.

3. The film thickness of the Alpharabola head was not as thick as that of the Alpharabola cup with the same equatorial radial clearance, while the maximum pressure of the Alpharabola head not as low as that of the Alpharabola cup.

4. The initial anteversion angle affected the lubrication performance of the nonspherical head prosthesis. However, compared with the lubrication improvement from the nonspherical bearing geometry, this effect was not significant.

ACKNOWLEDGEMENT

The authors would like to thank the Overseas Research Students Award Scheme (ORSAS) to Qingen Meng and the National Natural Science Foundation of China through grant 50628505. This work is also partly supported by the NIHR (National Institute for Health Research) as part of collaboration with the LMBRU (Leeds Musculoskeletal Biomedical Research Unit). John Fisher receives a Senior Investigator Award from the NIHR. This work was also supported by EPSRC and the Wellcome Trust through WELMEC the Centre of Excellence in Medical Engineering.

REFERENCES

[1] **Firkins, P. J., Tipper, J. L., Saadatzadeh, M. R., Ingham, E., Stone, M. H., Farrar, R.,** and **Fisher, J.** Quantitative analysis of wear and wear debris from metal-on-metal hip prostheses tested in a physiological hip joint simulator. *Bio-Medical Materials and Engineering*, 2001, **11(2)**, 143–157.

[2] **Catelas, I., Medley, J. B., Campbell, P. A., Huk, O. L.,** and **Bobyn, J. D.** Comparison of *in vitro* with *in vivo* characteristics of wear particles from metal-metal hip implants. *Journal of Biomedical Materials Research Part B: Applied Biomaterials*, 2004, **70(B2)**, 167–178.

[3] **Dobbs, H. S.** and **Minski, M. J.** Metal-ion release after total hip-replacement. *Biomaterials*, 1980, **1(4)**, 193–198.

[4] **Jacobs, J. J., Skipor, A. K., Doorn, P. F., Campbell, P., Schmalzried, T. P., Black, J.,** and **Amstutz, H. C.** Cobalt and chromium concentrations in patients with metal on metal total hip replacements. *Clinical Orthopaedics and Related Research*, 1996, **329**, S256–S263.

[5] **Skipor, A. K., Campbell, P. A., Patterson, L. M., Amstutz, H. C., Schmalzried, T. P.,** and **Jacobs, J. J.** Serum and urine metal levels in patients with metal-on-metal surface arthroplasty. *Journal of Materials Science: Materials in Medicine*, 2002, **13(12)**, 1227–1234.

[6] **Grubl, A., Marker, M., Brodner, W., Giurea, A., Heinze, G., Meisinger, V., Zehetgruber, H.,** and **Kotz, R.** Long-term follow-up of metal-on-metal total hip replacement. *Journal of Orthopaedic Research*, 2007, **25(7)**, 841–848.

[7] **Brown, C., Fisher, J.,** and **Ingham, E.** Biological effects of clinically relevant wear particles from metal-on-metal hip prostheses. *Proceedings of the Institution of Mechanical Engineers, Part H: Journal of Engineering in Medicine*, 2006, **220(H2)**, 355–369.

[8] **Cobb, A. G.** and **Schmalzreid, T. P.** The clinical significance of metal ion release from cobalt–chromium metal-on-metal hip joint arthroplasty. *Proceedings of the Institution of Mechanical Engineers, Part H: Journal of Engineering in Medicine*, 2006, **220(H2)**, 385–398

[9] **Bhamra, M. S.** and **Case, C. P.** Biological effects of metal-on-metal hip replacements. *Proceedings of the Institution of Mechanical Engineers, Part H: Journal of Engineering in Medicine*, 2006, **220(H2)**, 379–384

[10] **Anissian, H. L., Stark, A., Good, V., Dahlstrand, H.,** and **Clarke, I. C.** The wear pattern in metal-on-metal hip prostheses. *Journal of Biomedical Materials Research, Part B: Applied Biomaterials*, 2001, **58(B6)**: 673–678.

[11] **Rieker, C., Schon, R., Konrad, R., Liebentritt, G., Gnepf, P., Shen, M., Roberts, P.,** and **Grigoris, P.** Influence of the clearance on *in-vitro* tribology of large diameter metal-on-metal articulations pertaining to resurfacing hip implants. *Orthopedic Clinics of North America*, 2005, **36(2)**, 135–142.

[12] **Vassiliou, K., Elfick, A. P., Scholes, S. C.,** and **Unsworth, A.** The effect of 'running-in' on the tribology and surface morphology of metal-on-metal Birmingham hip resurfacing device in simulator studies. *Proceedings of the Institution of Mechanical Engineers, Part H: Journal of Engineering in Medicine*, 2006, **220(H2)**, 269–277.

[13] **Liu, F., Jin, Z. M., Hirt, F., Rieker, C., Roberts, P.,** and **Grigoris, P.** Effect of wear of bearing surfaces on elastohydrodynamic lubrication of metal-on-metal hip implants. *Proceedings of the Institution of Mechanical Engineers, Part H: Journal of Engineering in Medicine*, 2005, **219(H5)**, 319–328.

[14] **Lee, R., Essner, A.,** and **Wang, A.** Tribological considerations in primary and revision metal-on-metal arthroplasty. *The Journal of Bone and Joint Surgery, American Volume*, 2008, **90 (Suppl 3)**, 118–124.

[15] **Hu, X. Q., Isaac, G. H.,** and **Fisher, J.** Changes in the contact area during the bedding-in wear of different sizes of metal on metal hip prostheses. *Bio-Medical Materials and Engineering*, 2004, **14(2)**, 145–149.

[16] **Tuke, M. A., Scott, G., Roques, A., Hu, X. Q.,** and **Taylor, A.** Design considerations and life prediction of metal-on-metal bearings: the effect of clearance. *The Journal of Bone and Joint Surgery, American Volume*, 2008, **90 (Suppl 3**), 134–141.

[17] **Smith, S. L., Dowson, D.,** and **Goldsmith, A. A. J.** The lubrication of metal-on-metal total hip joints: a slide down the Stribeck curve. *Proceedings of the Institution of Mechanical Engineers, Part J: Journal of Engineering Tribology*, 2001, **215(J5)**, 483–493.

[18] **Dowson, D., Hardaker, C., Flett, M.,** and **Isaac, G. H.** A hip joint simulator study of the performance of metal-on-metal joints, Part II: design. *Journal of Arthroplasty*, 2004, **19(8)**, S124–S130.

[19] **Liu, F., Jin, Z. M., Roberts P.,** and **Grigoris, P.** Importance of head diameter, clearance, and cup wall thickness in elastohydrodynamic lubrication analysis of metal-on-metal hip resurfacing prostheses. *Proceedings of the Institution of Mechanical Engineers, Part H: Journal of Engineering in Medicine*, 2006, **220(H6)**, 695–704.

[20] **Farrar, R.** and **Schmidt, M. B.** The effect of diametral clearance on wear between head and cup for metal on metal articulations. No. 71, 43rd Annual Meeting of the Orthopaedic Research Society, 1997.

[21] **Shen, M. C., Rieker, C. B., Gnepf, P., Liebentritt, G.,** and **Schon, R.** Effect of clearance on frictional torque characteristics of metal-on-metal THA. No. 1196, 51st Annual Meeting of the Orthopaedic Research Society, 2005.

[22] **Jin, Z. M., Meakins, S., Morlock, M. M., Parsons P., Hardaker, C., Flett, M.,** and **Isaac, G.** Deformation of press-fitted metallic resurfacing cups. part 1: experimental simulation. *Proceedings of the Institution of Mechanical Engineers, Part H: Journal of Engineering in Medicine*, 2006, **220(H2)**, 299–309.

[23] **Meng, Q. E., Gao, L. M., Liu, F., Yang, P. R., Fisher, J.,** and **Jin, Z. M.** Contact mechanics and elastohydrodynamic lubrication in a novel metal-on-metal hip implant with an aspherical bearing Surface. *Journal of Biomechanics*, 2009, DOI: 10. 1016 / j. jbiomech. 2009. 11. 018.

[24] **Meng, Q. E., Gao, L. M., Liu, F., Yang, P. R., Fisher, J.,** and **Jin, Z. M.** Transient elastohydrodynamic lubrication analysis of a novel metal-on-metal hip prosthesis with an aspherical acetabular bearing surface. *Journal of Medical Biomechanics*, 2009, **24 (5)**, 352−362.

[25] **Hardaker, C., Dowson, D., and Isaac, G. H.** Head replacement, head rotation, and surface damage effects on metal-on-metal total hip replacements: a hip simulator study. *Proceedings of the Institution of Mechanical Engineers, Part H: Journal of Engineering in Medicine*, 2006, **220(2)**, 209−217.

[26] **Ernsberger, C. N.** and **Frazee, E. W.** Low ion release aspheric metal on metal hip design. No. 1788, 54th Annual Meeting of the Orthopaedic Research Society, 2008.

[27] **Lippincott, A. L.** and **Medley, J. B.** Low wear ball and cup joint prosthesis. United States Patent, US6059830, 5 May 2000.

[28] **Farrar, R.** and **Bigsby, R.** An orthopaedic joint prosthesis. WIPO Patent, WO 02/43626 A1, 6 June 2002.

[29] **Wang, F. C.** and **Jin, Z. M.** Transient elastohydrodynamic lubrication of hip joint implants. *Transaction of the ASME, Journal of Tribology*, 2008, **130(1)**: 011007.

[30] **Jagatia, M.** and **Jin, Z. M.** Elastohydrodynamic lubrication of metal-on-metal hip prostheses under steady state entraining motion. *Proceedings of the Institution of Mechanical Engineers, Part H: Journal of Engineering in Medicine*, 2001, **215(H6)**, 531–541.

[31] **Cooke, A. V., Dowson, D.,** and **Wright, V.** The rheology of synovial fluid and some potential synthetic lubricants for degenerate synovial joints. *Engineering in Medicine*, 1978, **7**, 66–72.

[32] **Yao, J. Q., Laurent, M. P., Johnson, T. S., Blanchard, C. R.,** and **Crowinshield, R. D.** The influence of lubricant and material on polymer/CoCr sliding friction. Wear, 2003, **255**, 780 –784.

[33] **Jin, Z. M.** Theoretical studies of elastohydrodynamic lubrication of artificial hip joints. *Proceedings of the Institution of Mechanical Engineers, Part J: Journal of Engineering Tribology*, 2006, **220(J8)**, 719–727.

[34] **Bergmann, G., Deuretzbacher, G., Heller, M., Graichen, F., Rohlmann, A., Strauss, J.,** and **Duda, G. N.** Hip contact forces and gait patterns from routine activities. *Journal of Biomechanics*, 2001, **34(7)**, 859–871.

[35] **Calonius, O.** and **Saikko, V.** Slide track analysis of eight contemporary hip simulator designs. *Journal of Biomechanics*, 2002, **35(11)**, 1439–1450.

[36] **ISO 14242-1.** Implants for surgery — wear of total hip-joint prostheses — Part 1: loading and displacement parameters for wear-testing machines and corresponding environmental conditions for test. 2002.

[37] **Gao, L. M., Wang, F. C., Yang, P. R.,** and **Jin, Z. M.** Effect of 3D physiological loading and motion on elastohydrodynamic lubrication of metal-on-metal total hip replacements. *Medical Engineering & Physics*, 2009, **31(6)**, 720**–**729.

[38] **Venner, C. H.** Multigrid solution of the EHL line and point contact problems. PhD thesis, University of Twente, Enschede, The Netherlands, 1991.

[39] **Liu, F., Jin, Z. M., Hart, F., Rieker, C.,** and **Roberts, P.** Transient elastohydrodynamic lubrication analysis of metal-on-metal hip implant under simulated walking conditions. *Journal of Biomechanics*, 2006, **39(5)**, 905–914.

[40] **Dowson, D.** and **Jin, Z. M.** Metal-on-metal hip joint tribology. *Proceedings of the Institution of Mechanical Engineers, Part J: Journal of Engineering Tribology*, 2006, **220(2)**, 107–118.

[41] **Tepic, S.** Wear-reducing geometry of articulations in total joint replacements. WIPO Patent, WO 2008/058756 A2, 22 May 2008.

Notation

e_x, e_y	eccentricities of the femoral head from the centre of the cup (m)
f_x, f_y, f_z	calculated load components (N), defined in equation (4)
h	film thickness (m)
p	pressure (Pa)
R_1	radius of femoral head for spherical hip prostheses; desired maximum radius of the Alpharabola head (m)
R_2	radius of the cup (m)
$R_{a(cup)}$	average roughness of the cup (m)
$R_{a(head)}$	average roughness of the head (m)
R_h	varying radius of femoral head (m)
t	time (s)
$T_{2,1}$	transformation matrix from the reference to the fixed coordinate systems
w_y	applied load in the y direction (N)
x, y, z	fixed Cartesian coordinates on the cup
x', y', z'	reference Cartesian coordinates fixed on the head
α	parameter controlling the variation rate of the radius of head
γ	rotation angle of the head
δ	elastic deformation of bearing surfaces (m)
η	viscosity of synovial fluid (Pa s)
Λ	lambda ratio, defined in equation (9)
ϕ, θ	angular coordinates in the entraining and side-leakage directions

	respectively
ω	angular velocity (rad/s)

Captions

Table 1 Typical geometric and mechanical parameters adopted for the EHL models of the MOM hip prostheses using an Alpharabola head

Fig. 1 A simple ball-in-socket configuration for the MOM hip prosthesis employing an Alpharabola head

Fig. 2 Variation in the dynamic load (a), velocity and rotation angle of the head (b) within a walking gait specified by the ISO standard

Fig. 3 Definition of spherical coordinates and mesh grid on a given level

Fig. 4 Predicted central and minimum film thicknesses (a) and maximum pressure (b) for a MOM hip prosthesis using an Alpharabola head during four walking cycles ($R_1 = R_2 = 14$ mm, $\alpha = 1.01$)

Fig. 5 Film thickness profiles and pressure distributions of a MOM hip prosthesis using an Alpharabola head at 0.1 s (a), 0.3 s (b) and 0.58 s (c) within a convergent cycle ($R_1 = R_2 = 14$ mm, $\alpha = 1.01$)

Fig. 6 Detailed variation in the lubricant film and hydrodynamic pressure at the central line along the entraining direction at different instants of one walking gait for an Alpharabola head hip prosthesis ($R_1 = R_2 = 14$ mm, $\alpha = 1.01$)

Fig. 7 Variation in the radial clearances at the loaded centre of the cup ($\theta = \pi/2$, $\phi = \pi/2$) during one walking gait for two Alpharabola head designs ($R_1 = R_2 = 14$ mm)

Fig. 8 Comparison of the central film thickness (a), minimum film thickness (b) and maximum pressure (c) between the MOM hip prostheses using an

Alpharabola head ($R_1 = R_2 = 14$ mm, $\alpha = 1.0043$), an Alpharabola cup ($R_1 = R_2 = 14$ mm, $\alpha = 0.9957$) and spherical bearing ($R_1 = 14$ mm, $R_2 = 14.03$ mm)

Fig. 9 Effect of the anteversion angle on the central film thickness (a), minimum film thickness (b) and maximum pressure (c) of a MOM hip prosthesis using a Alpharabola head ($R_1 = R_2 = 14$ mm, $\alpha = 1.0043$)

Table 1. Typical geometric and mechanical parameters adopted for the EHL models of the MOM hip prostheses using an Alpharabola head

Thickness of the equivalent support layer	2 mm
Wall thickness of the cup	9.5 mm
α	1.01, 1.0043
R_2	14 mm
R_1	14 mm
Elastic modulus of CoCr	210 GPa
Elastic modulus of the equivalent support layer	2.27 GPa
Poisson's ratio of CoCr	0.3
Poisson's ratio of the equivalent support layer	0.23
Viscosity of synovial fluid	0.002 Pas

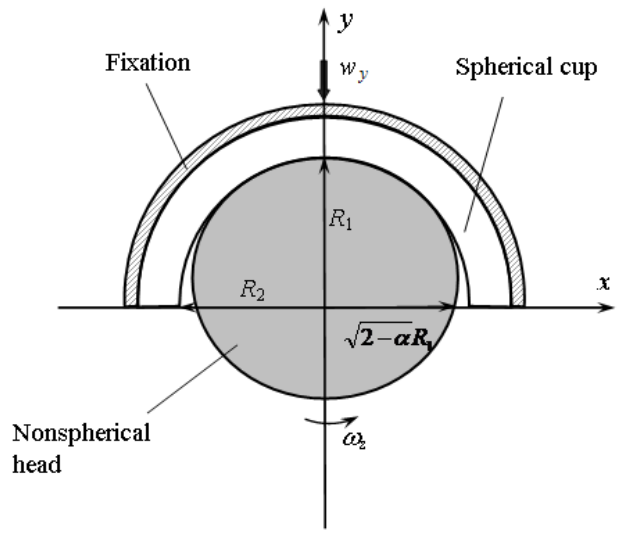

Fig. 1 A simple ball-in-socket configuration for the MOM hip prosthesis employing an Alpharabola head

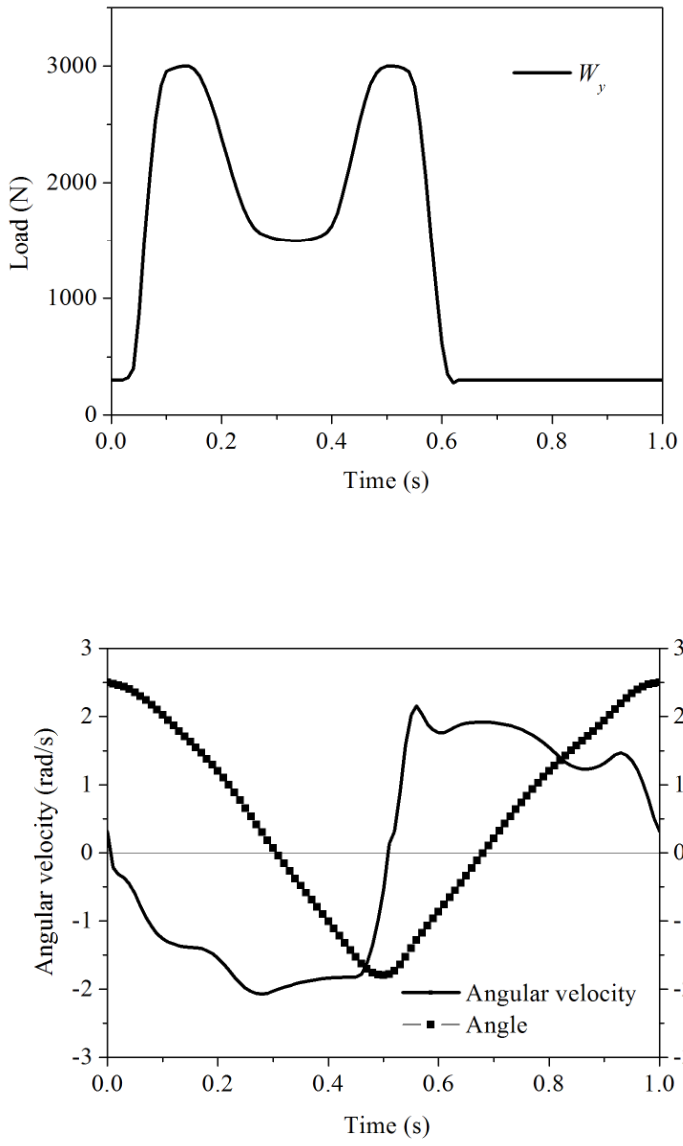

Fig. 2 Variation in the dynamic load (a), velocity and rotation angle of the head (b) within a walking gait specified by ISO standard

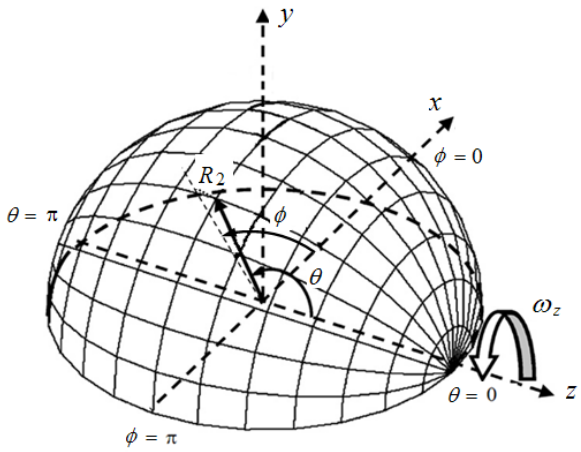

Fig. 3 Definition of spherical coordinates and mesh grid on a given level

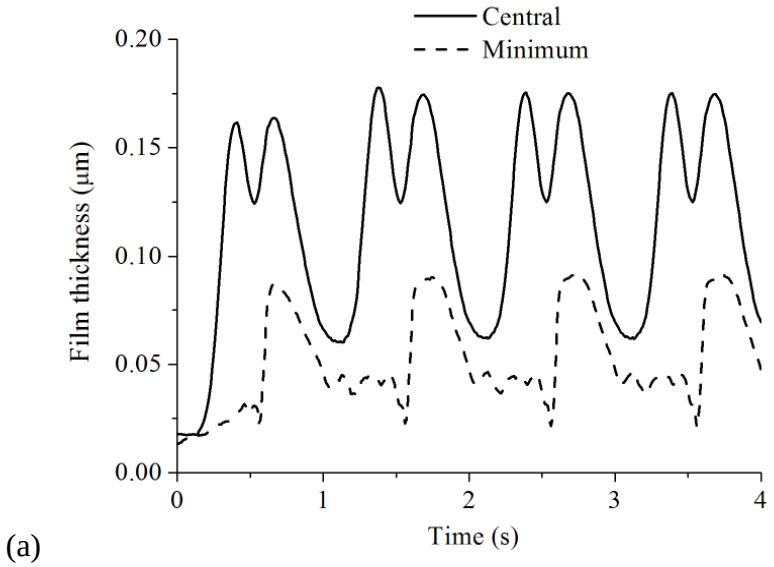

(a)

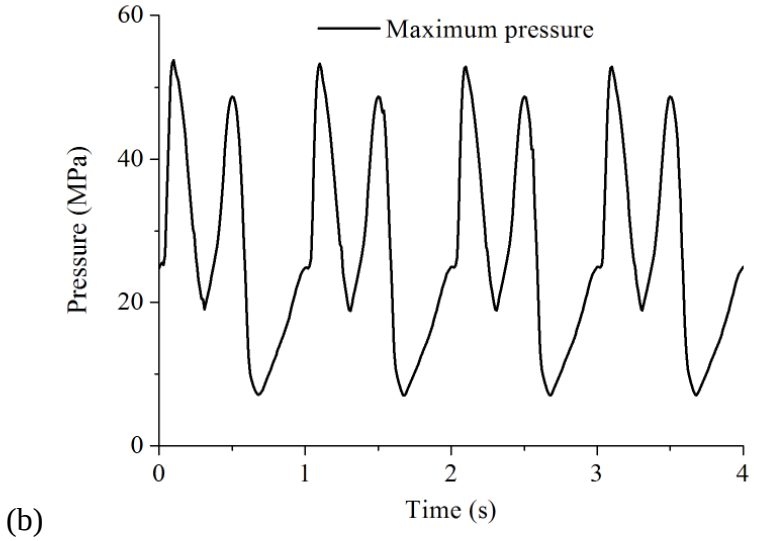

(b)

Fig. 4 Predicted central and minimum film thicknesses (a) and maximum pressure (b) for a MOM hip prosthesis using an Alpharabola head during four walking cycles (R_1 = R_2 = 14 mm, α = 1.01)

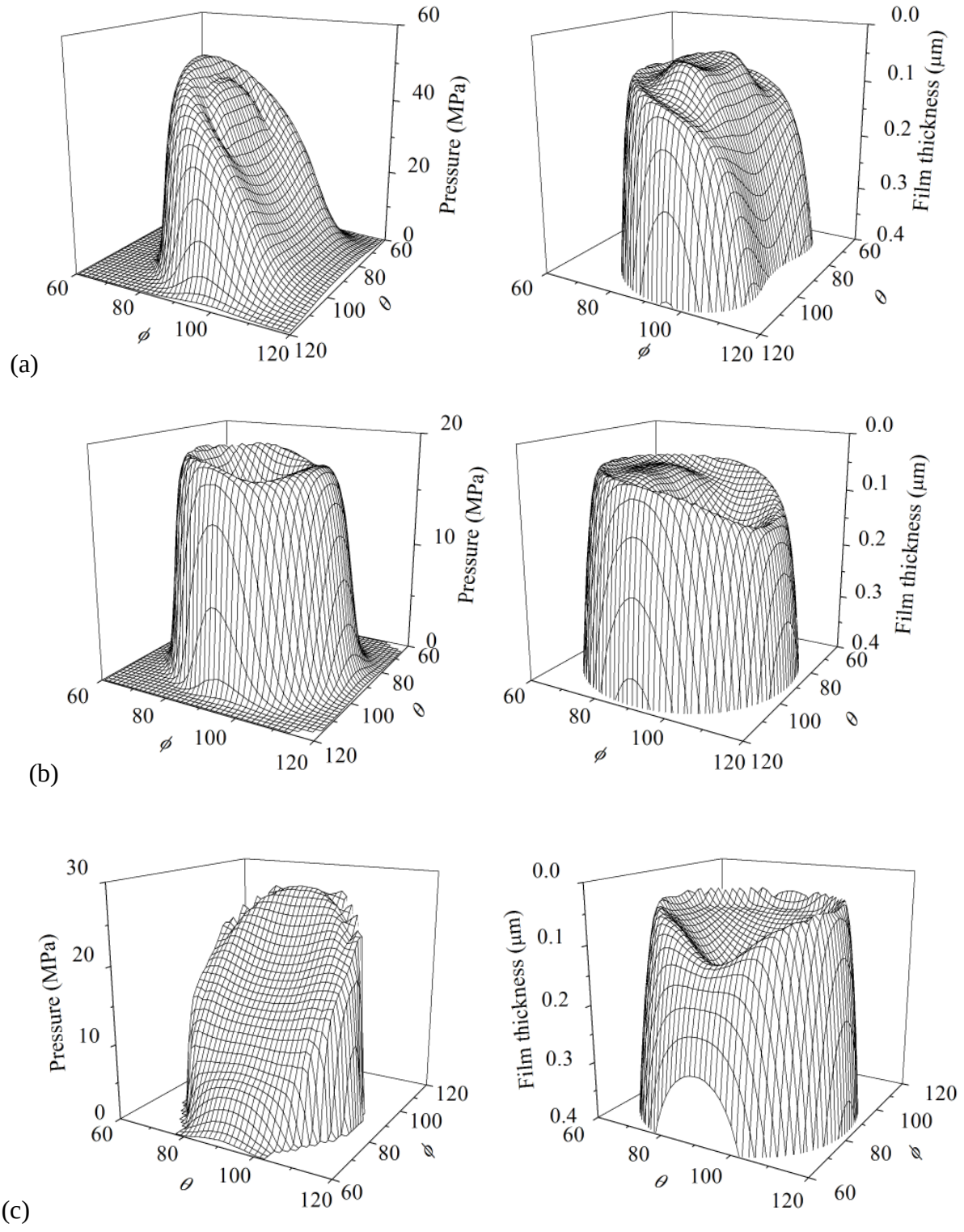

Fig. 5 Film thickness profiles and pressure distributions of a MOM hip prosthesis using an Alpharabola head at 0.1 s (a), 0.3 s (b) and 0.58 s (c) within a convergent cycle ($R_1 = R_2 = 14$ mm, $\alpha = 1.01$)

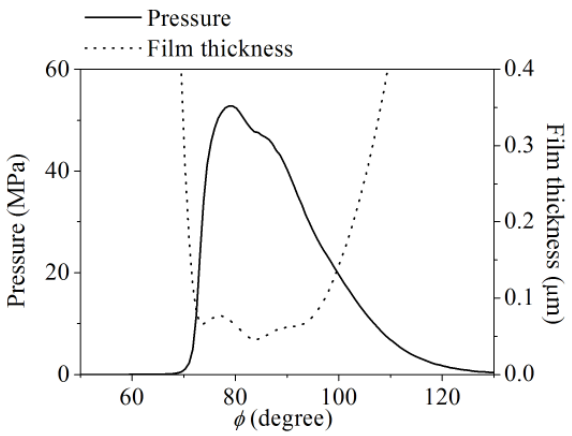

0.1 s

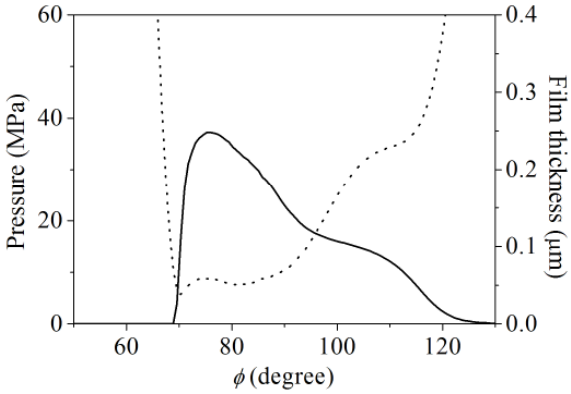

0.2 s

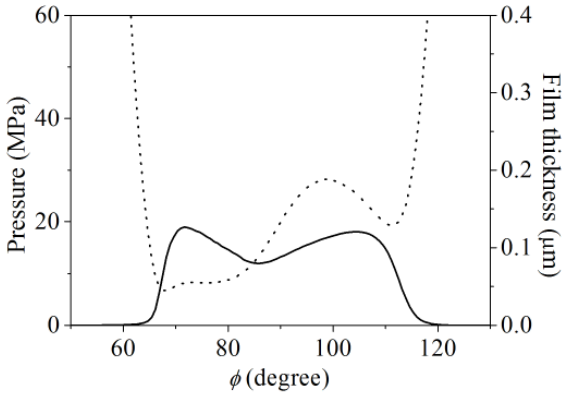

0.3 s

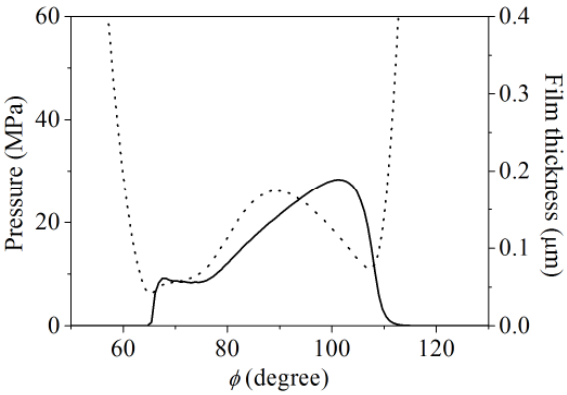

0.4 s

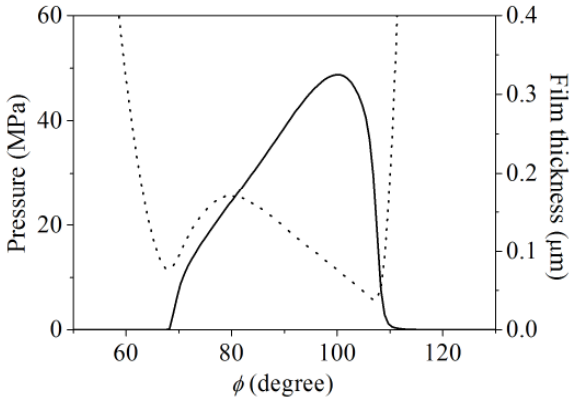

0.5 s

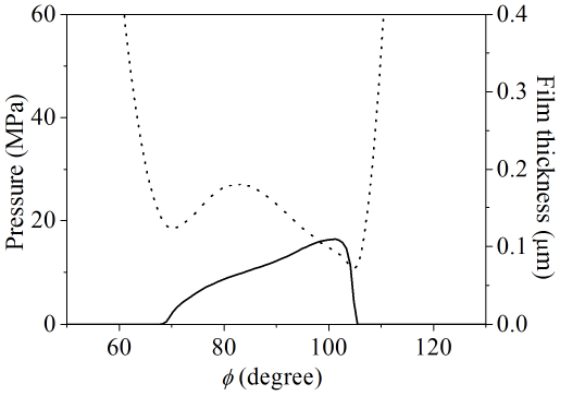

0.6 s

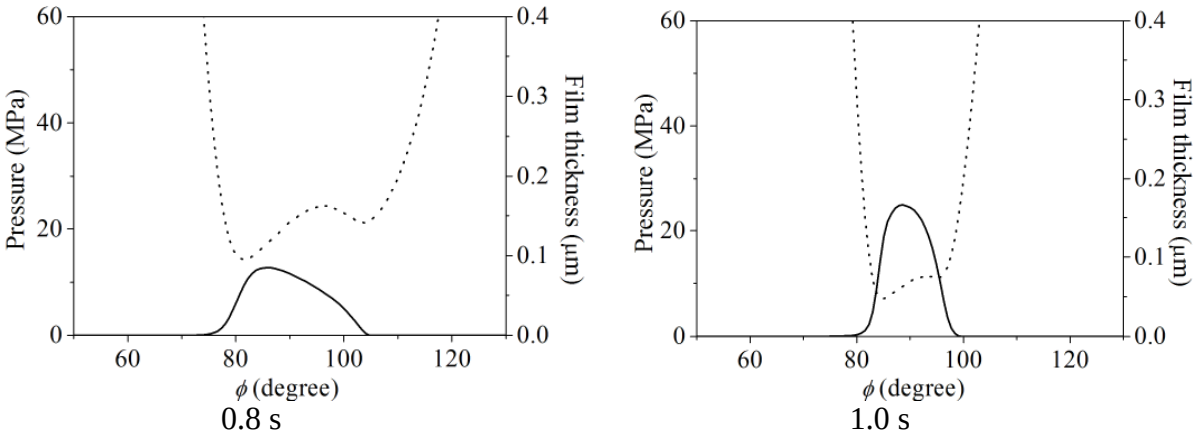

Fig. 6 Detailed variation in the lubricant film and hydrodynamic pressure at the central line along the entraining direction at different instants of one walking gait for an Alpharabola head hip prosthesis ($R_1 = R_2 = 14$ mm, $\alpha = 1.01$)

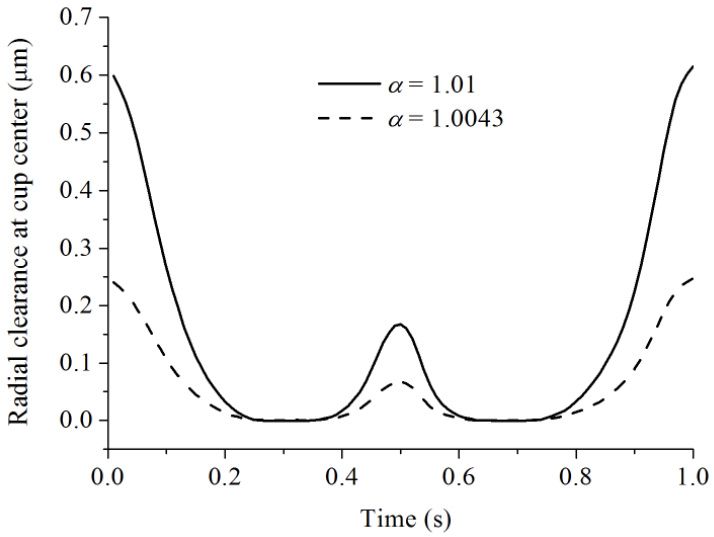

Fig. 7 Variation in the radial clearances at the loaded centre of the cup ($\theta = \pi/2$, $\phi = \pi/2$) during one walking gait for two Alpharabola head designs ($R_1 = R_2 = 14$ mm)

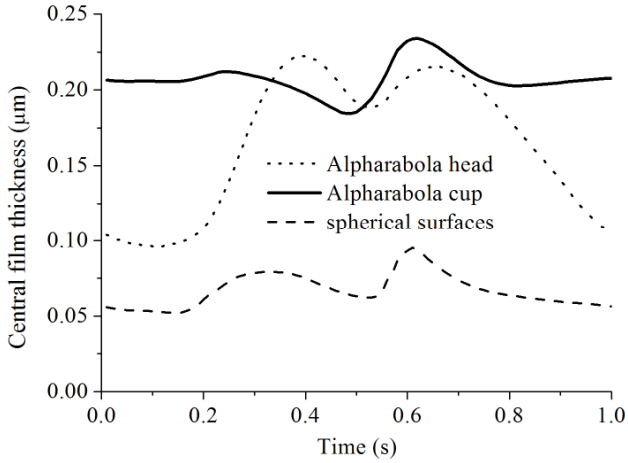

(a)

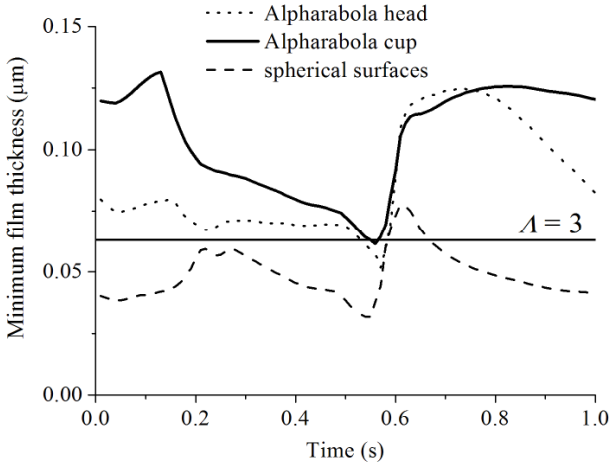

(b)

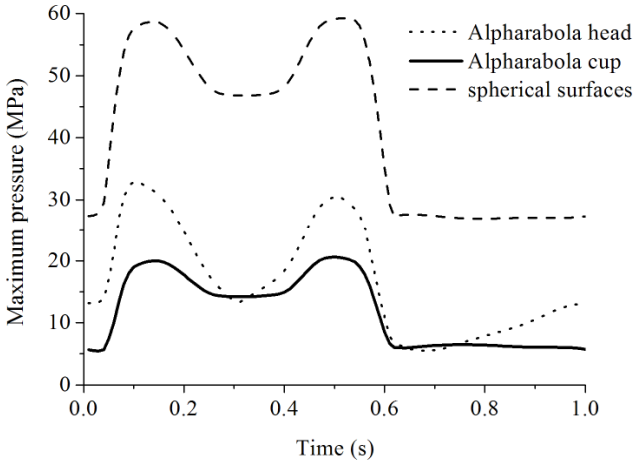

(c)

Fig. 8 Comparison of the central film thickness (a), minimum film thickness (b) and maximum pressure (c) between the MOM hip prostheses using an Alpharabola head (R_1 = R_2 = 14 mm, α = 1.0043), an Alpharabola cup (R_1 = R_2 = 14 mm, α = 0.9957) and spherical bearing (R_1 = 14 mm, R_2 = 14.03 mm)

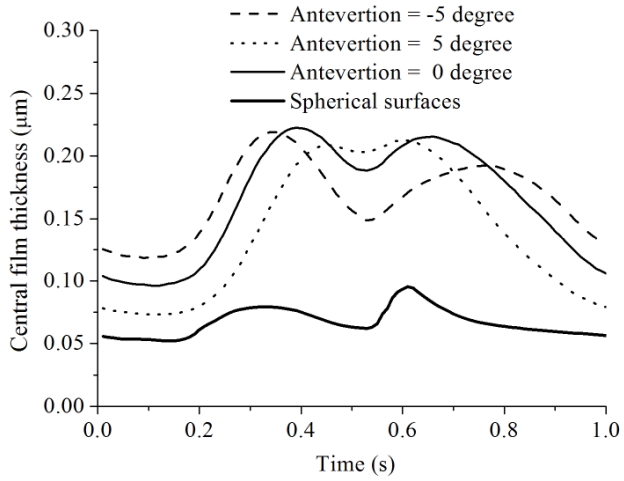

(a)

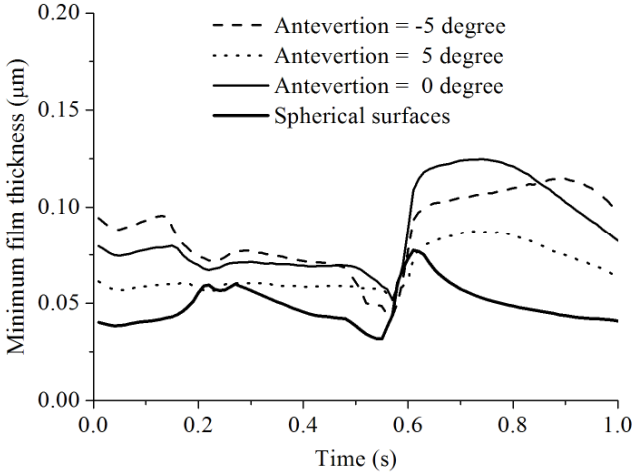

(b)

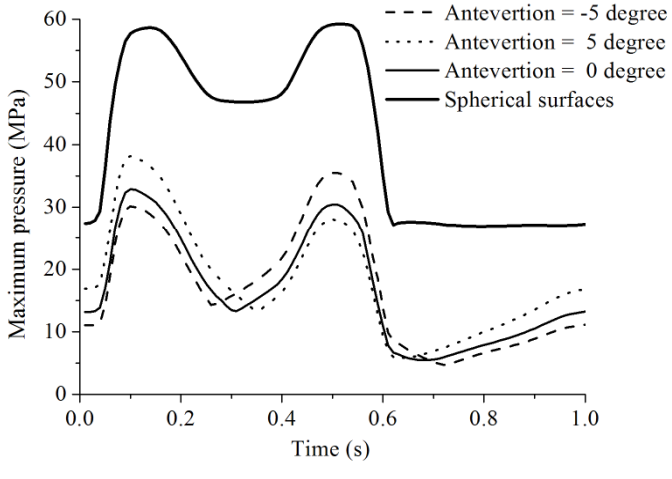

(c)

Fig. 9 Effect of the anteversion angle on the central film thickness (a), minimum film thickness (b) and maximum pressure (c) of a MOM hip prosthesis using a Alpharabola head ($R_1 = R_2 = 14$ mm, $\alpha = 1.0043$)